ACS APPLIED ELECTRONIC MATERIALS

pubs.acs.org/acsaelm

Article

Interplay between Optical and Electronic Characteristics of Castor Oil-Derived Hybrid Polymers

Francis D. R. Garcia,[‖] Edgar F. Pinzón Nieto,[‖] Bruno Seiki Domingos Onishi, Ricardo Bortoletto-Santos, Beatriz Damasio de Freitas, Adriano dos Santos, Danilo Manzani,* Paulo Roberto Bueno, and Sidney José Lima Ribeiro

Cite This: *ACS Appl. Electron. Mater.* 2025, 7, 8034−8044

Read Online

ACCESS | Metrics & More | Article Recommendations | Supporting Information

ABSTRACT: This work explores the correlation between information obtained from optical and electrochemical spectroscopy—specifically impedance-derived electrochemical capacitance spectroscopy (ECS)—applied to castor oil-derived hybrid polymers. The organic−inorganic hybrid polyurethane, called t-urethanesil_CO, was synthesized via a mild, catalyst-free sol−gel route and characterized by using FTIR spectroscopy, ^{29}Si nuclear magnetic resonance, and thermogravimetric analyses. ECS analysis provided unprecedented information about the electronic structure of t-urethanesil_CO through the chemical capacitance (C_q) response as a function of the applied potential, which is proportional to the experimental pseudocapacitive density of states (DOS). A Gaussian-shaped DOS profile was observed, characteristic of noncrystalline materials. Furthermore, light-assisted ECS—performed under continuous photoirradiation—revealed an enhancement in the C_q response, attributed to electron occupancy of excited states, consistent with the population of excited states under photoirradiation. To further investigate the optical-electronic interplay, the polymer was doped with photoactive polyoxometalate $H_3PW_{12}O_{40}$ (HPWA). The resulting PWA@t-urethanesil_CO exhibited potential shifts in the C_q profile and the emergence of new features under light-assisted ECS, indicating the formation of new electronic states within the polymer matrix arising from strong interactions with the dopant and their reduced specie W^{5+}, respectively. These findings highlight light-assisted ECS as a powerful in situ probe of the electronic structure in optically active hybrid materials.

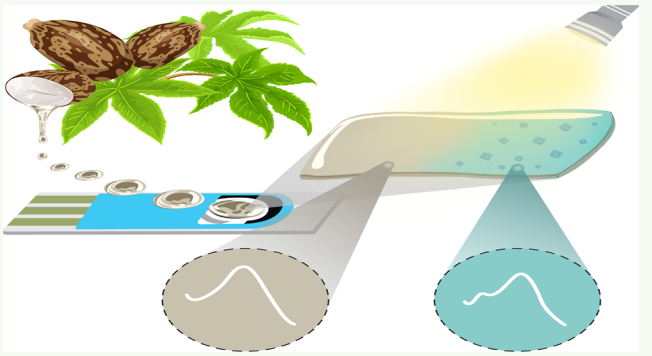

KEYWORDS: *urethanesil, polyoxometalate, photochromism, electronic structure, impedance-derived electrochemical capacitance spectroscopy*

INTRODUCTION

Polymers derived from renewable sources are highly desirable owing to their biodegradability, which significantly reduces their environmental impact when compared to conventional fossil-based polymers. Among the available sustainable resources for polymer production, vegetable oils stand out as a compelling choice due to their widespread availability in nature, cost-effectiveness, and versatile applications, such as coated fertilizers,[1,2] tissue regeneration membranes,[3] biolubrification, as well as metal removal.[4] In this context, castor Oil (CO) is a natural vegetable oil classified as a triglyceride ester, extracted from the seeds of *Ricinus communis* L (Euphorbiaceae family), commonly known as the castor plant. Academic and industrial interest in this natural oil has experienced significant growth. According to Ma et al.,[5] global production of CO stands at 500.000 tons annually. Notably, prominent companies such as BASF and Ford have already utilized CO derivatives in the development of foams-based materials, as highlighted by Singh et al.[6]

The unique structural composition of CO, characterized by the presence of hydroxyl groups (−OH), contributes to its enhanced solubility in polar solvents, increased viscosity, and chemical stability.[7−9] These attributes position CO as a promising candidate for eco-friendly polymer synthesis. Furthermore, −OH groups enable various reactions, mainly with an isocyanate group (−N═C═O), facilitating the formation of polyurethanes ($[-HN-COO-]_n$).

Polyurethanes based on CO find applications in bioadhesives,[10] surface coating for wood and steel,[11] and coating for corrosion resistance[12] and fertilizers.[2,13] While CO-based

Received: April 23, 2025
Revised: August 12, 2025
Accepted: August 13, 2025
Published: August 28, 2025

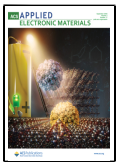

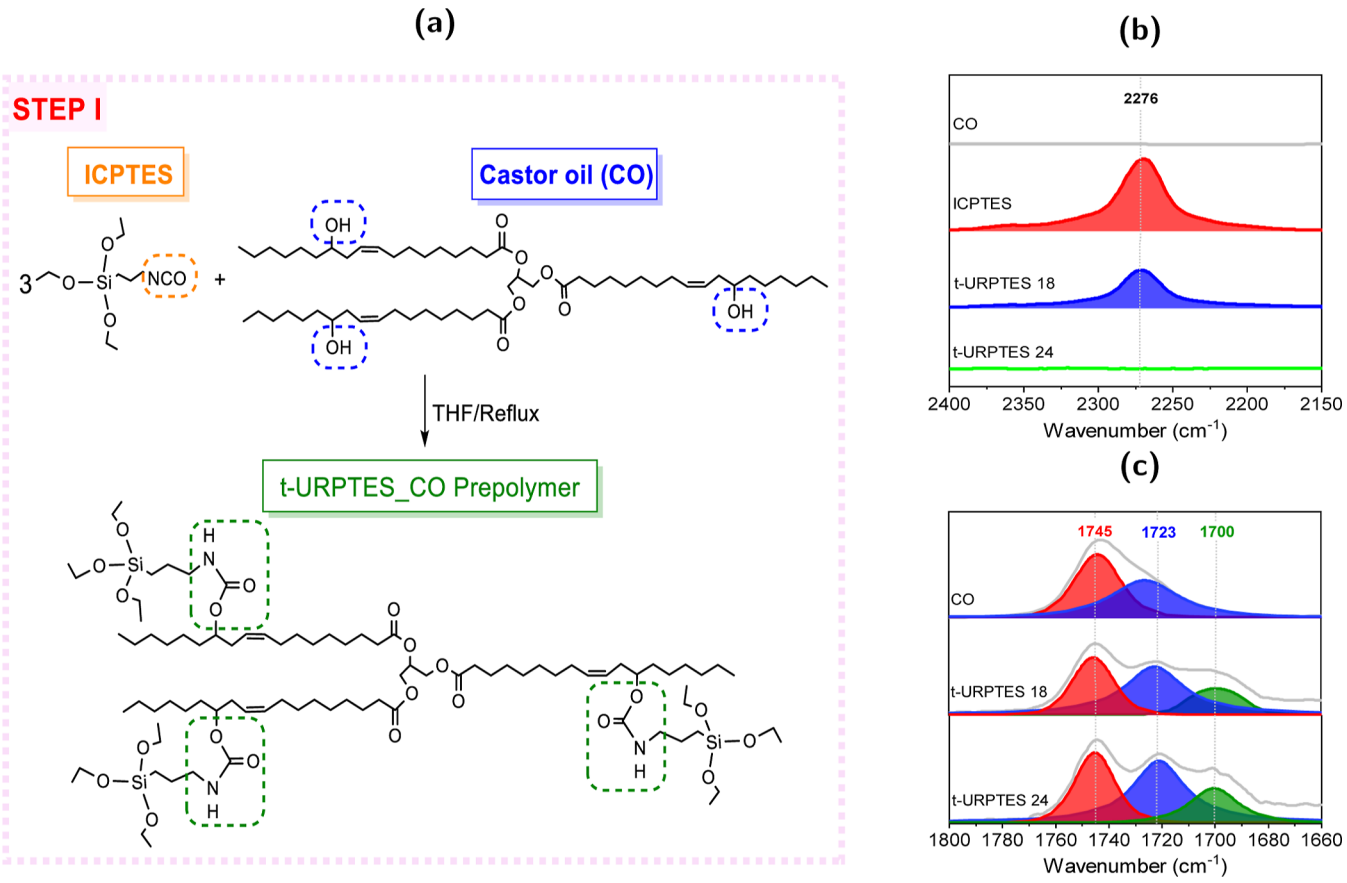

Figure 1. (a)Formation reaction of the t-urethanesilpropyltriethoxysilane (t-URPTES_CO) prepolymer. FTIR spectra (b) in the range of 2000−2400 cm^{-1} and (c) in the carbonyl absorption region of CO, ICPTES, and t-URPTES_CO after 18 and 24 h of reaction.

polyurethanes exhibit remarkable attributes such as hydrophobicity, adhesion, thermal stability,[14] and hardness,[15] they typically suffer from limited flexibility and lack of transparency, which can hinder their application in fields like photonics and optoelectronics. To overcome this limitation, Becchi and collaborators[12] developed organic−inorganic polymer films, commonly referred as organic−inorganic hybrid films, by incorporating CO with 3-aminopropyltriethoxysilane (APTES) and tetraethoxysilane for various coating applications. Their work demonstrated excellent adhesion, hardness, and, notably, transparency. Several other studies have also explored the integration of alkoxysilanes with CO in the development of organic−inorganic polymers films;[16−19] however many of these researches have not provided clear guidance regarding photophysical and electronic properties that could lead applications in other fields of material science, such as photonics and optoelectronics devices. This limitation is significant as the performance of such devices largely depends on the understanding and control of these properties.

In this context, the present study aims to synthesize CO-derived hybrid polyurethanes, with a focus on the synthetic route, structural characterization, and evaluation of their optical and electronic properties through correlation between photoluminescence and electrochemical capacitance spectroscopy (ECS)—the latter being applied for the first time to a hybrid polymer of the urethanesil type. In a previous work, the sol−gel methodology was proposed as a viable strategy for obtaining CO-derived hybrid urethanesil.[20] Unlike conventional synthetic routes, this inorganic polymerization process eliminates the need for a catalyst, employs eco-friendly solvents such as water and ethanol, and involves fewer procedural steps. Furthermore, we introduce a recent electrochemical approach that enables the in situ measurement of the electronic density of states (DOS) of hybrid polyurethane structures by using a three-electrode conventional setup. This methodology is based on the measurement of the C_q-property of chemical structures and has been successfully employed to reveal the DOS of various nanomaterials, including copper oxide nanofilms,[21] CdTe quantum dots,[22] graphene,[23] and electroactive peptides[24] (see Section S1 of the Supporting Information for detailed information).

Additionally, for exploring advanced properties related to the photoelectronic features of this polymeric structure, we have also developed a light stimuli-responsive material by incorporating a photochromic compound into organic−inorganic polyurethane. Materials exhibiting photochromism demonstrate a reversible optical response to light and have a broad range of established and potential technological applications. These include optical lenses,[25,26] smart windows,[27,28] ultraviolet ray detection[29,30] blue dosimeters indoor environments,[31] and optical data storage.[32,33] Phosphotungstic acid ($H_3PW_{12}O_{40}$−HPWA), which is a well-known inorganic photochromic compound, is a polyoxometalate with photoreduction properties triggered by ultraviolet and near-visible light irradiation.[34−36] The optical response results from the reduction of W^{6+} to W^{5+}, followed by the potential occurrence of a photoinduced proton transfer.

https://doi.org/10.1021/acsaelm.5c00826
ACS Appl. Electron. Mater. 2025, 7, 8034−8044

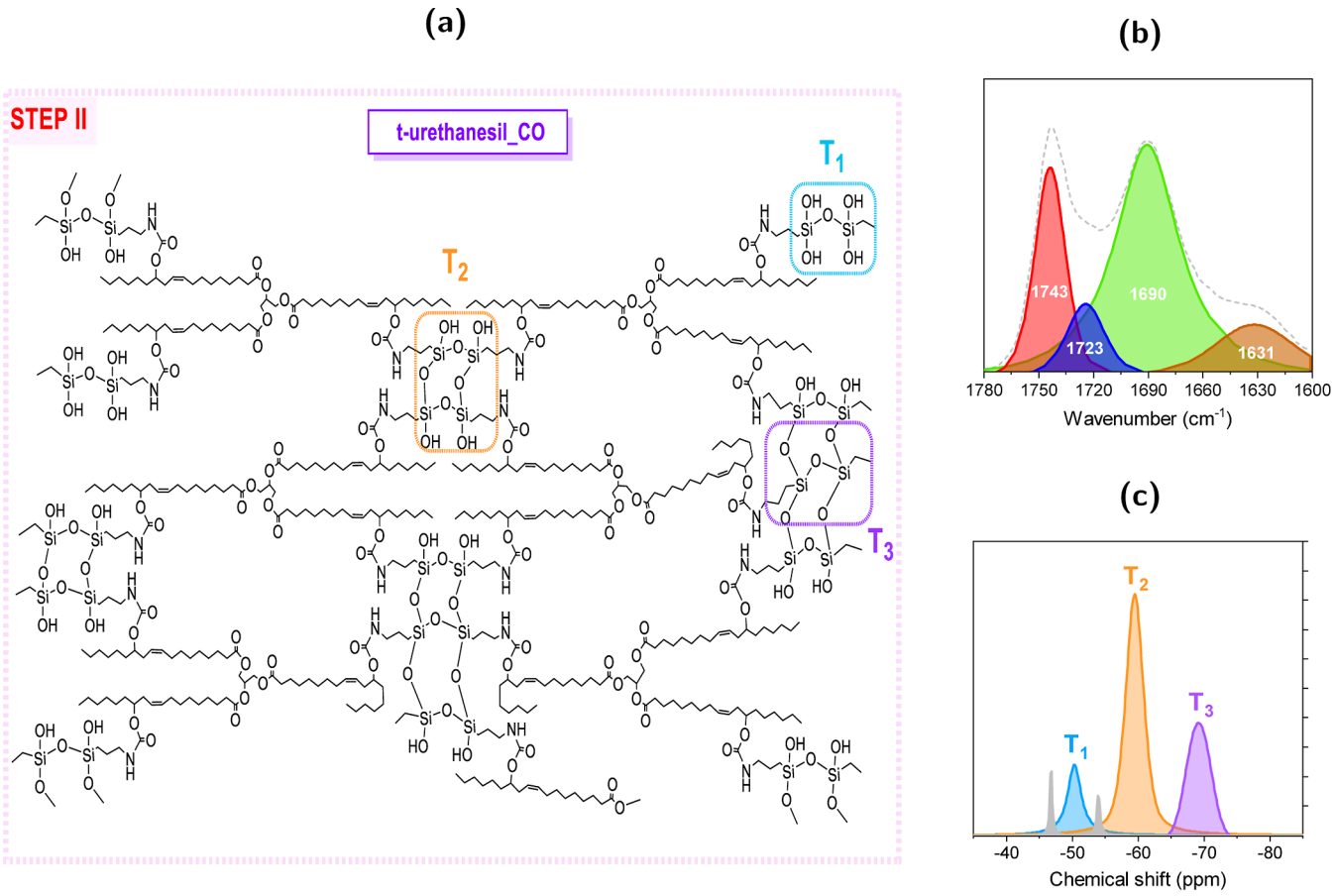

Figure 2. (a)Schematic representation of hybrid polymer network produced, t-urethanesil_CO. (b) FTIR spectrum at the carbonyl absorption region and (c) ^{29}Si MAS NMR spectrum of t-urethanesil_CO, showing T_1 (14.90%), T_2 (56.01%) and T_3 (24.55%) units.

The metastable chemical species, commonly referred to as "tungsten bronze", then absorbs visible light through d−d transition and intervalence charge−transfer transition (IVCT $W^{5+} \rightarrow W^{6+}$).[34−36] When the matrix acts as a proton donor group, several authors have emphasized its crucial role in the stabilization and reversibility of the process, indicating that these materials depend critically on a strong interaction between the PWA polyanion and the neighboring proton donor groups.[35,37,38] In this context, we aim to embed HPWA into the CO organic−inorganic hybrid and to demonstrate, through characterization techniques, the significant interactions facilitated by the presence of −NH functional groups distributed within the network. In 2017, Cruz and collaborators[39] presented a related example of HPWA in hybrid polymer with −NH groups. They developed a photochromic material using recycled poly(ethylene terephthalate) (PET) as a substrate and an organic−inorganic hybrid based on Jeffamine-D230 and ICPTES. Their study demonstrated a photochromic response and an enhanced reversible behavior with increasing temperature in the PWA-doped hybrid host matrix.

In contrast, the present work provides compelling evidence of the interplay between the optical and electronic properties of doped CO-based hybrid polymers, which exhibit promising characteristics for the development of light-responsive films driven by photochromism and intrinsic photoluminescence. To reach these conclusions, an approach was employed that correlates insights obtained from optical spectroscopy and time-dependent techniques, including infrared and Raman spectroscopy, UV−vis and photoluminescence spectroscopy, and cyclic voltammetry and ECS. Notably, ECS was applied—for the first time—to assess the pseudocapacitive electronic DOS of these hybrid polymeric materials via C_q measurements. This study thus represents a valuable contribution to the development and electronic characterization of versatile organic−inorganic hybrid polymeric structures derived from naturally sourced compounds such as CO. The main findings from the synthesis and characterization of these innovative materials are presented in the following section.

RESULTS AND DISCUSSION

CO-Based Triurethanesil Film [t-urethanesil_CO]. This section examines the structural properties of the t-urethanesil_CO film and its intermediates and provides relevant insights into the photophysical processes involved, based on electrochemical and electronic characterization of this polymer structure.

A significant advantage of this study is the synthesis of an organic−inorganic hybrid under mild conditions, utilizing low-toxicity solvents and a catalyst-free process through the sol−gel methodology. This methodology is the highly favorable route for inorganic polymerization with alkoxysilanes due to its ability to be conducted at room temperature using either water or ethanol as a solvents. The formation of the silicon network relies on the hydrolysis and condensation of alkoxysilane precursors. Following hydrolysis, which is favored under acidic or basic conditions, consecutive condensation reactions occur,

https://doi.org/10.1021/acsaelm.5c00826
ACS Appl. Electron. Mater. 2025, 7, 8034−8044

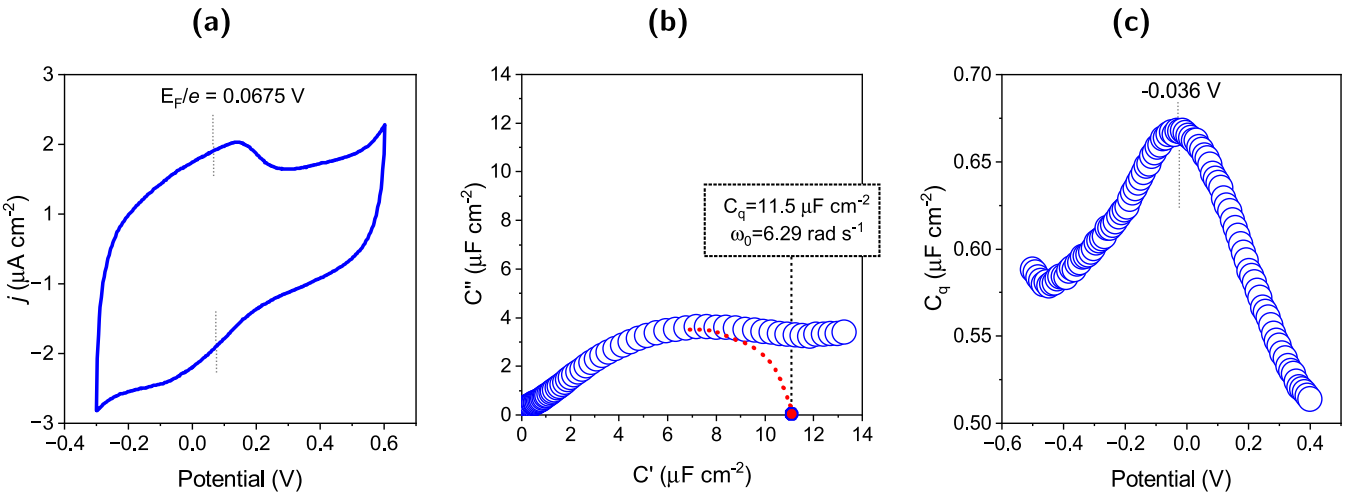

Figure 3. Electrochemical characterization of t-urethanesil_CO: (a) cyclic voltammogram (CV) using 0.2 mol L^{-1} H_2SO_4 as the electrolyte; (b) complex capacitive spectrum (Nyquist diagram) illustrating the film's response measured at the formal potential E_F/e; (c) profile of C_q-response as a function of the electrode potential ($\propto$ to the density-of-states function) of t-urethanesil_CO.

leading to the formation of siloxane composed of −Si−O−Si− linkages.[40−42]

As depicted in the condensation reaction illustrated in Figure 1a-Step I-, the (−N═C═O) group of 3-(isocyanatepropyl)triethoxysilane (ICPTES) reacts with −OH groups from glycerol triricinoleate (the major component in the composition of CO), leading to the formation of urethane bonds (−HN−COO−). The progression of this reaction was confirmed by FTIR spectroscopy (Figure 1b). Specifically, the disappearance of the 2276 cm^{-1} band after 24 h of reaction, attributed to the ν(−N═C═O) group, indicates the consumption of ICPTES.

Furthermore, the emergence of a new band in the carbonyl region suggested the formation of the urethane bond. The FTIR spectra at the carbonyl absorption region of CO and t-URPTES_CO after 18 and 24 h of the reaction exhibit a vibrational frequency at 1700 cm^{-1}, corresponding to stretching of the amide group ν(O═C−N−, amide I) (Figure 1c). The shift in the band around 1723 cm^{-1} may be attributed to the overlap of the urethane ester group's carbonyl vibration ν(O═C−O−) with other carbonyl functions present in CO, which also contribute to the band around 1745 cm^{-1}.[7,8]

Following the hydrolysis and condensation of the t-URPTES_CO polyurethane prepolymer, covalent bonds are formed between silanes (−Si−O−CH_2CH_3) present in the structure, resulting in the formation of an organic−inorganic polyurethane polymer with unique properties.

The formation of the organic−inorganic cross-linked t-urethanesil_CO via sol−gel is schematized in Figure 2a-Step II-. Deconvolution of the infrared absorption bands in the carbonyl region reveals three distinct bands (Figure 2b). In contrast to t-URPTES_CO, the band at 1690 cm^{-1} experienced a minor wavenumber shift, indicating hydrogen-bonded interurethane domains involving amide I (O═C−N−) and a lower energy shift of the urethane ester group (O═C−O−). Notably, an additional band is observed at 1631 cm^{-1}, attributed to an ordered hydrogen bond of amide I.[43]

Moreover, the polymerization of t-URPTES_CO through the (−Si−O−CH_2CH_3) groups was examined via solid-state NMR. The ^{29}Si magic angle spinning (MAS) NMR spectrum of t-urethanesil_CO displays distinct signals from the T_1 (δ −50.4 ppm), T_2 (δ −59.5 ppm), and T_3 (δ −69.3 ppm) environments (Figure 2c). The notation "T_n" (where n = 0, 1, 2 and 3) corresponds to the number of oxygen in the silicon bridge $R' - Si(-OSi)_n(OCH_2CH_3)_{3-n}$.

The polycondensation ratio of the organic−inorganic network, represented as c ($c = 1/3(\%T_1 + 2\ \%T_2 + 3\ \%T_3)$), was estimated from relative areas of the ^{29}Si NMR spectrum, resulting in a value of $c \approx 67\%$. This estimation indicated a dominance of T_2 units within the network, with a noncrystalline domain centered at $2\theta = 20°$, as shown in Figure S3a of the Supporting Information.[44−46] In the ^{29}Si NMR spectrum, narrow peaks at δ −46.8 and δ −54.0 ppm suggested possible residual monomers and oligomers following the condensation process. However, these remnants appear to have a negligible influence on the overall thermal stability of the network, as revealed by thermogravimetric analysis shown in Figure S3b. Details of the X-ray diffraction and thermogravimetric analyses are provided in Section S2 of the Supporting Information document.

Furthermore, electrochemical measurements were performed on the t-urethanesil_CO hybrid polymer with the primary aim of analyzing its electrochemical and electronic properties. Initially, cyclic voltammetry (CV) was conducted, revealing a capacitive response with a pair of quasi-reversible waves within the potential window ranging from −0.3 to +0.6 V versus silver (Figure 3a). These signals are believed to stem from the −NH component of the network structure, potentially undergoing electron-induced proton transfer (R−NH ⇆ $R-N^- + H^+ + e^-$).[47,48] Weak peaks in the CV response of the carbon electrode display significant changes in the electric current and potential after modification with the hybrid polymer (Figure S4a).

From the CV results, the formal potential was estimated to be E_F/e = 0.0675 V, which is the potential representing the midpoint of the redox waves and the equilibrium potential of the electrochemical process associated with them. Subsequently, ECS was conducted using this formal potential as the bias potential. The impedance-derived capacitance response is illustrated in a Nyquist plot, which depicts a semicircle-shaped response correlating the real component of the capacitance (C') with the imaginary component (C''). Figure 3b presents the Nyquist plot for t-urethanesil_CO, showing that C' at low

https://doi.org/10.1021/acsaelm.5c00826
ACS Appl. Electron. Mater. 2025, 7, 8034−8044

frequencies, graphically where the semicircle closes, is approximately 11.5 μF cm^{-2}. This capacitance, named electrochemical capacitance ($C_{\bar{\mu}}$), can be quantified in terms of the chemical capacitance C_q of the polymer structure, which has an electronic origin and characterizes the pseudocapacitive behavior of the polymeric film, including its redox activity. From the perspective of quantum rate theory (QRT),[49,50] in dynamic equilibrium conditions in an electrolyte environment, the electrostatic capacitance (C_e) contribution is equivalent to the chemical, such as $C_e \sim C_q$, and thus $C_{\bar{\mu}} \propto C_q$. In addition, the frequency associated with this capacitance is considered to be the equilibrium angular frequency (ω_0), which presently was measured as 6.29 rad s^{-1}. According to the experimental approach derived from QRT (Section S1 in the Supporting Information), ω_0 is the angular frequency at which the t-urethanesil_CO polymer films return close to their electronic equilibrium condition under electrical perturbation.

Likewise, C_q can be derived from the impedance data when the angular frequency associated with the complex capacitance function $C^*(\omega)$ tends to 0 ($\omega \to 0$), as described in Equation S2 of the Supporting Information. Under these conditions, C' at ω_0 correspond to C_q. Then, measurements were conducted at this constant frequency, $\omega_0 = 6.29$ rad s^{-1}, to observe the C_q-response as a function of the electrode potential (Figure 3c).

In that sense, C_q originates from a volumetric distribution of nanometer sites exhibiting redox activity, specifically involving electron transfer processes. Thus, it is appropriate to describe this capacitance as being associated with a pseudocapacitive electronic DOS within a micrometer-scale volume.[51,52] Accordingly, Figure 3c can be interpreted as a representation of the DOS of the polymeric material at room temperature. The plot reveals an asymmetric response, peaking at −0.036 V, corresponding to the energy state distribution of an assembly of molecular units composing the polymer films. This distribution takes into account the thermal broadening effect on the energy levels, following the relation $C_q \propto f(1 - f)$, where f is the Fermi−Dirac distribution. Notably, this profile type obtained from the C_q-response is predominantly associated with the theoretical description of the electronic structure in noncrystalline molecular solids.[53,54] Similarly, the in situ C_q-response was evaluated for the urethanesil_CO-modified working electrode under light exposure (λ of 405 nm and optical power of 64 mW) (Figure 4, red dot). This response maintained the same asymmetric profile but shifted toward higher C_q values. A noteworthy feature of t-urethanesil_CO is its optical responsiveness characterized by blue emission, as shown in (Figure S5b,d)—that is, under exposure to a specific light source, the electrons of the material are promoted to higher energy states and subsequently relax, emitting blue light—although 405 nm is not the maximum excitation wavelength, it still has sufficient energy to populate accessible excited states, as estimated in Section S4 of the Supporting Information.

Therefore, the increase in C_q, without a significant change in the overall profile shape, is attributed to the electron occupancy of pre-existing excited states that become accessible under illumination. From a theoretical perspective, the chemical capacitance C_q is directly proportional to the density of electronic states (DOS) near the Fermi level.[21] It reflects the number of energy states available for electron occupation. Thus, an increase in C_q indicates a higher density of accessible states involved in electrons redistribution processes—consistent with the population of excited states under photoirradiation.[55−57]

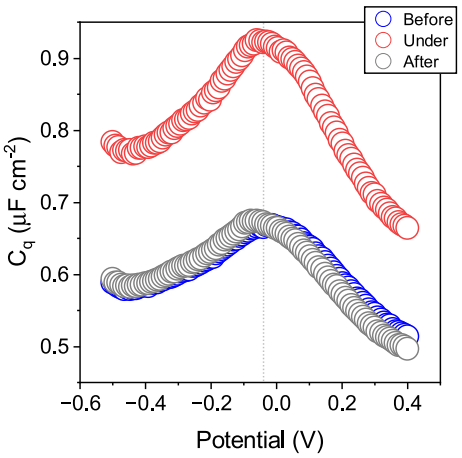

Figure 4. Profile of C_q-response as a function of the electrode potential (∝ to the density-of-states function) of t-urethanesil_CO before (blue circle), under (red circle), and after (blue circle) light irradiation with λ of 405 nm and optical power of 64 mW.

By observing the DOS response recorded under both conditions—without and with photoexcitation—it can be concluded that the observed changes in C_q are due to electron occupancy of excited states rather than the emergence of new states. This interpretation is further supported by the fact that no significant modifications in the profile shape were observed.

The correlation between optical excitation and C_q supports the interpretation of light-assisted ECS as a powerful in situ probe of the electronic structure in materials.

Notably, when the light is turned off (Figure 4, gray dot), the DOS profile is fully restored, demonstrating the reversible photodynamic behavior of the polymer structure. This behavior highlights the potential of the C_q response in t-urethanesil_CO as a promising signal for a logic system driven by physical stimuli, such as light, which can be translated into binary logic outputs (0 or 1).

Building on the previous findings, the next step of the study was to observe the behavior of the hybrid polymer when employed as a host matrix for intrinsically photosensitive materials such as photochromic species. The incorporation of these materials could enhance the polymer's light responsiveness and offer further confirmation of its electronic structure, as analyzed through ECS.

Smart Light-Responsive Film [PWA@t-Urethanesil_-CO]. The current section examines the changes in the electrochemical and electronic properties of t-urethanesil_CO upon incorporation of the dopant polyoxometalate $H_3PW_{12}O_{40}$−HPWA, referred to as PWA@t-urethanesil_CO. First, CV data presented in Figure 6a showed a significant increase in current density for PWA@t-urethanesil_CO compared to the undoped polymer, suggesting the preparation of a potential solid electrolyte from the doping of the polymer network. The homogeneous embedding of the HPWA was further supported by micrographs and elemental analysis via X-ray energy-dispersive spectroscopy (EDS) (Figure 5).

Upon estimation of E_F/e = 0.186 V, a Nyquist plot was obtained, revealing a notable increase in the value of the C_q-response (Figure 6b). Hence, from its semicircle-shaped response, it is possible to observe that the value of C_q was approximately (270 ± 50) μF cm^{-2}, which was calculated as

https://doi.org/10.1021/acsaelm.5c00826
ACS Appl. Electron. Mater. 2025, 7, 8034−8044

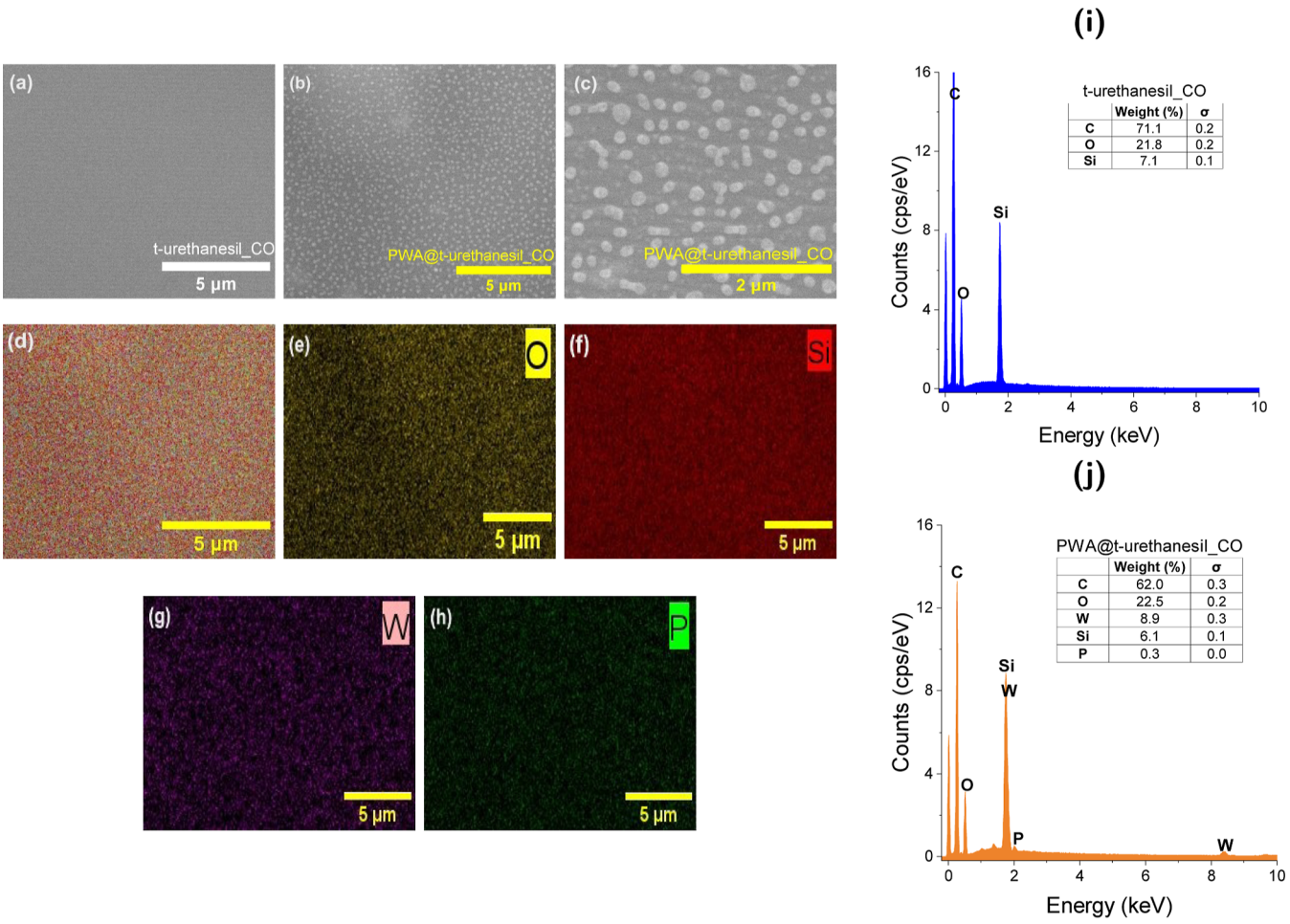

Figure 5. Scanning electron micrographs of (a) t-urethanesil_CO and (b,c) PWA@t-urethanesil_CO on the surface of the working electrode of screen-printed carbon electrodes (SPCEs). The morphology of the electrode surface after modification with the hybrid polymers is clearly observed. Additionally, the homogeneity of the HPWA doping is qualitatively demonstrated by the elemental mapping (d–h). (i,j) Semiquantitative elemental analysis by EDS. Theoretical weight percentage of tungsten: 7.6.

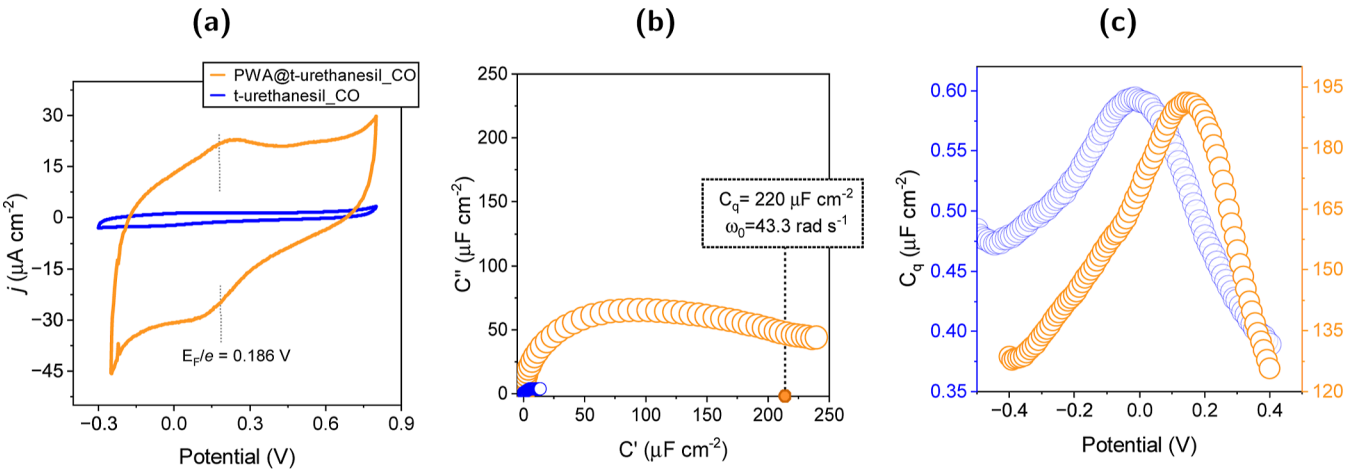

Figure 6. Electrochemical properties of PWA@t-urethanesil_CO (orange line): (a) cyclic voltammogram (CV) within the potential window of −0.3 to +0.8 V, (b) Nyquist diagram measured at the formal potential E_F/e, (c) profile of C_q-response as a function of the electrode potential (∝ to the density-of-states function) and compared with the host matrix (blue line).

the average of the three independent electrodes. This value is at least 20 times greater than that of t-urethanesil_CO, demonstrating the gaining of the pseudocapacitive features as a result of the doping. HPWA is a heteropolyacid containing metallic centers (W^{6+}) that participate in reversible redox reactions involving the transition between oxidation states of tungsten ($W^{6+} \leftrightarrows W^{5+}$). When the polymeric film is doped with HPWA, these redox-active centers are distributed

https://doi.org/10.1021/acsaelm.5c00826
ACS Appl. Electron. Mater. 2025, 7, 8034−8044

throughout its volume, giving rise to a pseudocapacitive effect.[58−60] This redox process contributes an additional component of electronic capacitance, which accounts for the significant increase in the electrochemical performance of the doped polymeric film.

In this case, the Nyquist plot also provided the equilibrium angular frequency, ω_0 = 43.3 rad s^{-1}, for PWA@t-urethanesil_CO. At this fixed ω_0, the C_q-response as a function of the electrode potential was obtained in the same electrolytic solution. As explained previously, this response is associated with the pseudocapacitive electronic DOS of the structure immobilized over the electrode.

Accordingly, Figure 6c shows an C_q-response with a maximum within the same potential window as t-urethanesil_CO when HPWA is embedded into the structure. In addition to the significant increase in magnitude, the response differs substantially from the undoped host, displaying a distinct shift of its maximum—corresponding to the Fermi-level of the structure—toward more positive potentials, 0.152 V. These changes in the C_q profile suggest a modified electronic structure of the polymer matrix, likely due to the emergence of new electronic states arising from interactions with the HPWA dopant.

Further evidence for this interaction between the PWA anion and the polymer host is provided by the FTIR spectrum of PWA@t-urethanesil_CO, particularly in the carbonyl absorption region, supporting the interaction of polyanion with the −NH moiety. In the undoped polymer, the amide I band—associated with strongly ordered hydrogen bonding—appears at 1631 cm^{-1}. Upon incorporation of the PWA anion into the hybrid matrix, this band exhibits a blue shift to 1665 cm^{-1} (Figure S6b). This shift is attributed to the formation of disordered hydrogen bonds between the amide I moieties and the oxygen atoms of the PWA anion. Such disordered interactions typically reduce the hydrogen bond strength, allowing greater vibrational freedom of the −C═O groups and consequently increasing their vibrational frequency.

Therefore, the structural correlation mentioned above suggests the possibility of evaluating the photophysical behavior of this doped polymer structure through light-assisted ECS, serving as a powerful in situ probe of the material's electronic structure.

Exposure of PWA@t-urethanesil_CO to light at λ = 405 nm resulted in the emergence of two characteristic absorption bands in the visible region (Figure 7a). The first band, appearing between 710 and 800 nm, is attributed to IVCT ($W_A^{5+}-O-W_B^{6+} \leftrightarrows W_A^{6+}-O-W_B^{5+}$). The second, higher energy band around 480 nm is assigned to d−d transition of new W^{5+} species due to the d^1 orbital.[61] The same light dose was used to collect the C_q-response versus potential plot (DOS), as presented in Figure 7b. It showed a shift of the original maximum toward higher values of C_q and lower potentials, 0.034 V. Additionally, a new contribution emerged at the negative potential, peaking at −0.027 V.

From C_q analyses, it is suggested that the new contribution arises from a polymer moiety interacting with a highly reduced PWA unit, such as $[PW_6^{5+}W_6^{6+}O_{40}]^{9-}$. The higher values of C_q (ranging from 192 to 233 $\mu F\ cm^{-2}$) indicate a process predominantly occurring within the polymer matrix, driven by the incorporation of the reduced PWA anion. This behavior is likely associated with electronic transitions involving newly formed states linked to W^{5+} centers as well as IVCT processes.

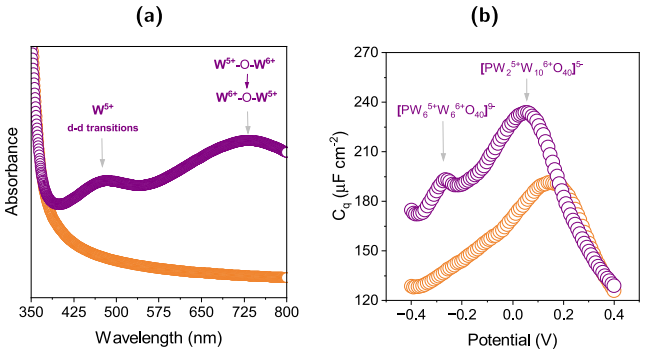

Figure 7. Optical and electronic characteristics of PWA@t-urethanesil_CO: (a) UV/vis spectrum; (b) profile of the C_q-response as a function of the electrode potential ($\propto$ to the density-of-states function), before (orange dots) and after (violet dots) irradiation exposure (λ = 405 nm; optical power = 64 mW).

The partial reduction of tungsten atoms in the PWA framework—manifested by the coexistence of W^{5+} and W^{6+}—may result in the shift of the electrochemical response of PWA@t-urethanesil_CO toward more negative potentials. Hence, the presence of a higher concentration of W^{5+} centers within the PWA structure appears to be correlated to more negative potential regions, reflecting enhanced redox activity within the hybrid material.

In this context, these results presented in Figure 8a,b also propose the PWA@t-urethanesil_CO-doped polymer as a potential material for data storage, with "0" representing the electronic structure without light exposure and "1" representing light exposure. The innovative aspect is that being a common chromism mediated by light, these changes can be evaluated through the experimental electronic structure obtained via ECS. Therefore, the kinetics of this response were analyzed. When assessing the relaxation of the photochromic process, both UV/vis spectroscopy and ECS indicate a decline in the reduced species W^{5+}. While UV/vis spectroscopy demonstrates a consistent tendency toward decreasing the electronic transitions triggered by W^{5+} presence, the DOS analysis reveals a relaxation behavior without a clear tendency to recover the initial electronic structure, at least until 300 min. Even an unknown process might be triggered during this relaxation time. Interestingly, a follow-up study conducted 1 week later on the same sample revealed that PWA@t-urethanesil_CO exhibits a partial recovery of its electronic structure (Figure S8). This doped polymer, derived from CO, shows potential for applications as a semireversible logic gate system using a light-assisted ECS response. Therefore, this approach—based on the correlation between information obtained from optical and electrochemical spectroscopic methodologies—can be considered a powerful tool for in situ exploring the electronic and photophysical properties of chemically complex systems such as photo-chromic or -active and polymer structures.

CONCLUSION

In summary, this study reported the synthesis of organic−inorganic hybrid polymers, namely, the undoped t-urethanesil_CO and its polyoxometalate-doped PWA@t-urethanesil_CO, via a catalyst-free sol−gel route. The use of biobased precursors as CO and mild processing conditions aligns well

https://doi.org/10.1021/acsaelm.5c00826
ACS Appl. Electron. Mater. 2025, 7, 8034−8044

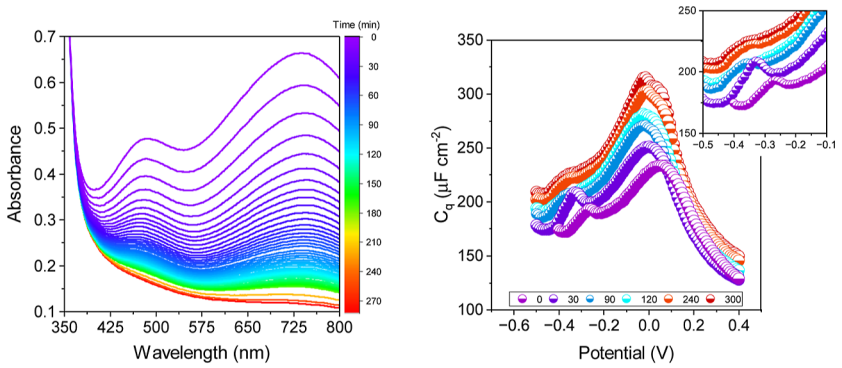

Figure 8. Evolution of the reversion of the photochromic process measured through (a) UV/vis spectra and (b) C_q-response with respect to the potential plot from 0 to 300 min.

with sustainable development goals, highlighting the potential of these materials for future green technologies.

Impedance-derived ECS provided the first experimental insights into the electronic structure of an organic−inorganic hybrid urethanesil. Moreover, the light-assisted ECS reveals the in situ population of excited electronic states, demonstrating its relevance as a probe of the electronic structure in optically active materials.

To further investigate the interplay between the optical and electronic properties of CO-derived hybrid polymers and to confirm their accessible electronic features, t-urethanesil_CO was embedded with the polyoxometalate HPWA—a distinct active compound based in photochromism. The resulting PWA@t-urethanesil_CO exhibited pronounced modifications in both ECS and light-assisted ECS profiles—such as potential shifts and the emergence of new features—indicative of new electronic states arising from strong interactions between the polymer and the PWA units and their reduced species.

All in all, these findings demonstrate that the combination of optical and electrochemical spectroscopies offers a robust in situ approach for probing the electronic and photophysical properties of complex systems, including photochromic, photoactive, and polymer-based materials. This strategy opens new avenues for experimentally accessing the electronic structure of optically active materials under ambient conditions.

EXPERIMENTAL SECTION

Materials. Castor oil (CO, supplied by A. Azevedo Brazil), (3-isocyanatepropyl)triethoxysilane (ICPTES, 95.0%, Sigma-Aldrich); tetrahydrofuran (THF, 99.9%, Sigma-Aldrich), ethanol (EtOH, 99.5%, Merck), hydrochloric acid (HCl, 37.0%, Merck), potassium chloride (KCl, 99.9%, Sigma-Aldrich), potassium hexacyanoferrate-(III) ($K_3[Fe(CN)_6]$, 99.0%, Sigma-Aldrich), and phosphotungstic acid hydrate ($HPWA−H_3PW_{12}O_{40}·H_2O$, 99.0%, Sigma-Aldrich) were used as reagents and solvents in their as-received state without further purification. Solutions were prepared with high-purity deionized water (Millipore, 18.2 MΩ cm at 25 °C). A phosphate buffer solution at pH 7, used as the supporting electrolyte, was prepared by dissolving disodium hydrogen phosphate dodecahydrate ($Na_2HPO_4·12H_2O$, 10 mmol L^{-1}, Sigma-Aldrich) and potassium dihydrogen phosphate (KH_2PO_4, 2 mmol L^{-1}, Sigma-Aldrich).

Methods. *Preparation of Triurethanesilpropyltriethoxysilane Prepolymer [t-URPTES_CO].* ICPTES was added to a mixture of CO in a 3:1 molar ratio with THF in a v/v ratio of THF/CO as 1:4. The mixture was heated under reflux and stirred for 24 h at 82 °C (thermostatic bath set as 17 °C). Following THF evaporation, t-URPTES_CO was obtained as a viscous pale-yellow liquid and then transferred to a covered glass bottle and stored at 10 °C away from direct light exposure.

Syntheses of a CO-Based Triurethanesil Film [t-urethanesil_CO] and Doped with Phosphotungstic Acid [PWA@t-Urethanesil_CO]. For the t-urethanesil_CO film, 3 g of the t-URPTES_CO prepolymer was mixed with 4 mL of EtOH and 200 μL of HCl 0.05 mol L^{-1} under stirring. The mixture was then poured into a polystyrene case and subjected to a heat treatment at 40 °C for 48 h. To produce PWA@t-UR_CO, 300 mg of PWA was solubilized in 4 mL of EtOH and added to 3 g of t-URPTES_CO.

FTIR-ATR Spectroscopy. Samples were analyzed using a spectrophotometer (Thermo Scientific Nicolet iS5) in the frequency range of 4000−600 cm^{-1}, with 32 scans and a spectral resolution of 2 cm^{-1}. The attenuated total reflectance module (Thermo Scientific iD3 ATR) integrated with a germanium crystal was employed.

Raman Spectroscopy. Raman spectra were obtained using a micro-Raman spectrometer (Horiba, LabRam HR Evolution) with excitation at a 633 nm laser. The spectra were collected in the wavenumber range of 600−1200 cm^{-1} with a spectral resolution of 1.2 cm^{-1}, using samples in both powder and films.

Solid-State Nuclear Magnetic Resonance. ^{29}Si magic-angle spinning (MAS) NMR spectra were collected by using a spectrometer (Bruker Avance III HD 400WB) equipped with a triple resonance probe at a spinning frequency of 10 kHz and a relaxation delay of 5 s. Integrated areas of signals were calculated by spectral deconvolution using PeakFit and Lorentzian−Gaussian as the band shape.

X-ray Powder Diffractometry. Diffraction pattern analysis was performed at room temperature using a diffractometer (Shimadzu LabX XRD6000) with 2θ ranging from 4° to 70°, at a step of 0.02° and 5° min^{-1} scanning rate. A Cu Kα radiation source (1.54184 Å) was used.

UV−Visible Spectroscopy. Absorbance spectra were recorded in the range of 250−800 nm using a UV/vis/NIR spectrophotometer (Agilent Varian Cary 5000) with samples approximately 1 mm thick. Transmission measurements were conducted by using a dual-beam UV/vis/NIR spectrophotometer (PerkinElmer Lambda 1050) equipped with a 150 mm integrating sphere accessory and a photomultiplier tube detector. For total transmission measurements, the film samples were mounted on the transmission port of the integrating sphere, with the (Spectralon USRS-99-020) reflectance standard placed on the backport. The diffuse transmission was recorded by removing the reflectance standard from the backport. Both total and diffuse transmission spectra were weighted by the CIE C standard spectral power density and integrated over the range of 380−780 nm. These values were subsequently used to calculate the haze factor (diffuse transmission/total transmission) and luminous transmittance (total transmission).[62,63]

Photoluminescence Spectroscopy. Excitation and emission spectra were measured at room temperature using a spectrofluorometer (Horiba Scientific Fluorologo-3 model FL3-22) in frontal-face acquisition mode. A 450 W xenon arc lamp served as an excitation

https://doi.org/10.1021/acsaelm.5c00826
ACS Appl. Electron. Mater. 2025, 7, 8034−8044

source. Emission spectra were recorded with an excitation wavelength of 320 nm over a spectral range of 350−750 nm, employing a 1 nm slit width and integration time of 0.2 s. The spectra were corrected for the photomultiplier's optical spectral response. Excitation spectra were obtained at an emission wavelength of 417 nm within the spectral range 250−400 nm using the same slit width and integration time. The spectra were adjusted for the lamp's spectral intensity distribution using a reference detector.

Thermogravimetry. Thermogravimetric curves were obtained using a TA Instruments TGA-Q500 module with a sample mass of 8.0 mg on a platinum crucible under an N_2 atmosphere at a flow rate of 60 mL min^{-1}. The temperature ranges from 30 to 800 °C with a heating rate of 10 °C min^{-1}.

Field Emission Gun Scanning Electron Microscopy. The micrographs were acquired as well as the X-ray EDS analyses were performed using a field emission scanning electron microscope (JEOL, JSM-IT500HR) equipped with a Schottky field emission gun, operating with an electron beam at 18 keV and a current of 0.17 nA. The samples were analyzed on the surface of the working electrode of SPCEs.

Electrochemical Measurements. The electrochemical experiments were performed using a portable potentiostat (PalmSens4) with a frequency response analyzer, adapted to a DSC connector for Screen-Printed Carbon Electrodes (SPCEs, Dropsens 110). The SPCEs consisted of a carbon working electrode (diameter 4 mm), a carbon counter electrode, and a silver pseudoreference electrode on ceramic substrates (length 33 mm; width 10 mm; height 0.5 mm). Activation of the SPCE's surface was reported by Saciloto et al.[64] using cyclic voltammetry (CV) between −1.0 and 1.5 V versus silver in 0.1 mol L^{-1} phosphate buffer solution pH 7, with a scan rate of 0.1 V s^{-1} until a stable signal was obtained (∼100 cycles). To confirm the electrochemical activation, CV was performed in 0.005 mol L^{-1} $K_3[Fe(CN)_6]$ in 0.5 mol L^{-1} KCl solution at the same scan rate. Postactivation, SPCEs were washed with high-purity deionized water and air-dried at room temperature. The working electrode was modified by coating with a viscous suspension of t-urethanesil_CO or PWA@t-urethanesil_CO using a glass rod of similar diameter and left to dry overnight at room temperature. The CV of the modified electrodes was carried out using 0.2 mol L^{-1} H_2SO_4 as the supporting electrolyte within a potential window of −0.3 to 0.4 V versus silver and a scan rate of 0.1 V s^{-1}.

Impedance-Derived Electrochemical capacitance spectroscopy. Measurements were performed by applying a sinusoidal potential bias equivalent to the formal potential of the interface, with a root-mean-square (RMS) potential amplitude $|V|$ of 10 mV over a potential bias V measured concerning the Fermi-level potential of the electrode. The frequency range scanned was from 1 MHz to 1 Hz, with the corresponding angular frequency ω calculated as $\omega = 2\pi f$, where f is the frequency in Hz. The capacitance response of the polymer film was obtained from the raw impedance data using the relation $C^*(\omega) = 1/j\omega Z^*(\omega)$, where $C^*(\omega)$ and $Z^*(\omega)$ represent the complex capacitance and impedance functions, respectively, ω is the angular frequency, and j is the imaginary unity $j = \sqrt{-1}$. Real (C') and imaginary (C'') capacitance components were obtained using the equations $C' = Z''/(\omega|Z|^2)$ and $C'' = Z'/(\omega|Z|^2)$, where Z' and Z'' corresponds to the real and imaginary impedance components, and $|Z|$ is the impedance modulus. In this sense, the response of chemical capacitance (C_q) of the interface corresponds to the value of C' as the frequency tends to zero or graphically in the capacitive Nyquist plot (C'' vs C') at the value of C' where the semicircle-shaped response closes. Additionally, impedance measurements were recorded for a fixed angular frequency ω_0, associated with C_q and while sweeping the potential from −0.5 to 0.4 V vs the silver electrode. This aimed to examine the variation of C_q concerning the potential, which allows access to the pseudocapacitive electronic density-of-states (DOS) of the polymer interface, as explained in more detail in Section S1 of the Supporting Information document.

■ ASSOCIATED CONTENT

Supporting Information

The Supporting Information is available free of charge at https://pubs.acs.org/doi/10.1021/acsaelm.5c00826.

Quantum rate spectroscopy as a tool to access to the electronic density-of-states; structural analyses and thermal stability of the undoped polymer t-urethanesil_CO film; electrochemical characterization of activated SPCE; optical properties of the t-urethanesil_CO film; structural and optical characterization of doped hybrid polymer PWA@t-urethanesil_CO; and photokinetic of PWA@t-urethanesil_CO through impedance-derived ECS (PDF)

■ AUTHOR INFORMATION

Corresponding Author

Danilo Manzani − *São Carlos Institute of Chemistry, University of São Paulo, IQSC-USP, 13560-970 São Carlos, Brazil;* orcid.org/0000-0001-7280-5404; Email: dmanzani@usp.br

Authors

Francis D. R. Garcia − *São Carlos Institute of Chemistry, University of São Paulo, IQSC-USP, 13560-970 São Carlos, Brazil*

Edgar F. Pinzón Nieto − *Institute of Chemistry, São Paulo State University, IQ-UNESP, 14800-060 Araraquara, Brazil*

Bruno Seiki Domingos Onishi − *São Carlos Institute of Chemistry, University of São Paulo, IQSC-USP, 13560-970 São Carlos, Brazil*

Ricardo Bortoletto-Santos − *University of Ribeirão Preto, UNAERP, 14096-900 Ribeirão Preto, Brazil;* orcid.org/0000-0002-4447-8239

Beatriz Damasio de Freitas − *Institute of Chemistry, São Paulo State University, IQ-UNESP, 14800-060 Araraquara, Brazil*

Adriano dos Santos − *Institute of Chemistry, São Paulo State University, IQ-UNESP, 14800-060 Araraquara, Brazil;* orcid.org/0000-0001-6812-5609

Paulo Roberto Bueno − *Institute of Chemistry, São Paulo State University, IQ-UNESP, 14800-060 Araraquara, Brazil;* orcid.org/0000-0003-2827-0208

Sidney José Lima Ribeiro − *Institute of Chemistry, São Paulo State University, IQ-UNESP, 14800-060 Araraquara, Brazil;* orcid.org/0000-0002-8162-6747

Complete contact information is available at: https://pubs.acs.org/10.1021/acsaelm.5c00826

Author Contributions

‖F.D.R.G. and E.F.P.N. contributed equally. **Francis D. R. Garcia**: Conceptualization, Methodology, Investigation, Visualization, Writing—original draft. **Edgar F. Pinzon Nieto**: Conceptualization, Methodology, Visualization, Writing—original draft. **Bruno Seiki Onishi**: Conceptualization, Writing—original draft. **Ricardo Bortoletto-Santos**: Conceptualization, Methodology. **Beatriz Damasio de Freitas**: Methodology. **Adriano Dos Santos**: Conceptualization, Supervision. **Danilo Manzani**: Resources, Funding acquisition, Supervision and Review. **Paulo Roberto Bueno**: Resources, Methodology, Supervision, Funding acquisition, Review and Editing. **Sidney José Lima Ribeiro**: Resources, Funding acquisition, Supervision.

https://doi.org/10.1021/acsaelm.5c00826
ACS Appl. Electron. Mater. 2025, 7, 8034−8044

Funding

The Article Processing Charge for the publication of this research was funded by the Coordenacao de Aperfeicoamento de Pessoal de Nivel Superior (CAPES), Brazil (ROR identifier: 00x0ma614).

Notes

The authors declare no competing financial interest.

■ ACKNOWLEDGMENTS

This work was supported by the National Council for Scientific and Technological Development (CNPq), under grant no. 405048/2021-1, no. 159320/2019-4, no. 2023/15384-0, no. 304718/2023-8 and no. 140351/2022-1. Additional support was provided by the São Paulo Research Foundation (FAPESP) through grant no. 2023/07987-7, no. 2017/24839-0, no. 2021/08111-2, no. 2024/03721-5, no. 2024/02000-2, and no. 2025/03273-5. B.S.D.O. acknowledges financial support from SISFOTON-MCTI (grant no. 440217/2021-0). S. J. L.R. also expresses gratitude to the Brazilian Networks INCT National Institute of Photonics and the INCT National Institute Nanomaterials for Life.

■ REFERENCES

(1) Yuan, S.; Cheng, L.; Tan, Z. Characteristics and preparation of oil-coated fertilizers: A review. *J. Controlled Release* **2022**, *345*, 675−684.
(2) Bortoletto-Santos, R.; Ribeiro, C.; Polito, W. L. Controlled release of nitrogen-source fertilizers by natural-oil-based poly(urethane) coatings: The kinetic aspects of urea release. *J. Appl. Polym. Sci.* **2016**, *133*, 43790.
(3) Ribeiro, A. R.; Silva, S. S.; Reis, R. L. Challenges and opportunities on vegetable oils derived systems for biomedical applications. *Biomater. Adv.* **2022**, *134*, 112720.
(4) Cubero-Cardoso, J.; Cuadri, A. A.; Fermoso, F. G.; Martín-Alfonso, J. E.; Urbano, J. Promising Chalcogenide Hybrid Copolymers for Sustainable Applications as Bio-lubricants and Metal Adsorbents. *ACS Appl. Polym. Mater.* **2022**, *4*, 3667−3675.
(5) Ma, Y.; Wang, R.; Li, Q.; Li, M.; Liu, C.; Jia, P. Castor oil as a platform for preparing bio-based chemicals and polymer materials. *Green Mater.* **2022**, *10*, 99−109.
(6) Singh, S.; Sharma, S.; Sarma, S. J.; Brar, S. K. A comprehensive review of castor oil-derived renewable and sustainable industrial products. *Environ. Prog. Sustainable Energy* **2023**, *42*, 14008.
(7) Ristić, I. S.; Budinski-Simendić, J.; Krakovsky, I.; Valentova, H.; Radičević, R.; Cakić, S.; Nikolić, N. The properties of polyurethane hybrid materials based on castor oil. *Mater. Chem. Phys.* **2012**, *132*, 74−81.
(8) Chauke, N. P.; Mukaya, H. E.; Nkazi, D. B. Chemical modifications of castor oil: A review. *Sci. Prog.* **2019**, *102*, 199−217.
(9) Ogunniyi, D. S. Castor oil: a vital industrial raw material. *Bioresour. Technol.* **2006**, *97*, 1086−1091.
(10) Ferreira, P.; Pereira, R.; Coelho, J. F. J.; Silva, A. F. M.; Gil, M. H. Modification of the biopolymer castor oil with free isocyanate groups to be applied as bioadhesive. *Int. J. Biol. Macromol.* **2007**, *40*, 144−152.
(11) Valero, M. F.; Ortegón, Y. Polyurethane elastomers-based modified castor oil and poly(ϵ-caprolactone) for surface-coating applications. *J. Elastomers Plast.* **2015**, *47*, 360−369.
(12) Becchi, D. M.; de Luca, M. A.; Martinelli, M.; Mitidieri, S. Organic−inorganic coatings based on epoxidised castor oil/APTES/TEOS. *J. Am. Oil Chem. Soc.* **2011**, *88*, 101−109.
(13) Bortoletto-Santos, R.; Plotegher, F.; Majaron, V. F.; da Silva, M. G.; Polito, W. L.; Ribeiro, C. Polyurethane nanocomposites can increase the release control in granulated fertilizers by controlling nutrient diffusion. *Appl. Clay Sci.* **2020**, *199*, 105874.
(14) Gama, N.; Ferreira, A.; Barros-Timmons, A. Cure and performance of castor oil polyurethane adhesive. *Int. J. Adhes. Adhes.* **2019**, *95*, 102413.
(15) Macalino, A. D.; Salen, V. A.; Reyes, L. Q. Castor oil based polyurethanes: Synthesis and characterization. *IOP Conf. Ser.: Mater. Sci. Eng.* **2017**, *229*, 012016.
(16) Parvathy, P. A.; Sahoo, S. K. Hydrophobic, moisture resistant and biorenewable paper coating derived from castor oil based epoxy methyl ricinoleate with repulpable potential. *Prog. Org. Coat.* **2021**, *158*, 106347.
(17) Akram, D.; Hakami, O.; Sharmin, E.; Ahmad, S. Castor and Linseed oil (polyurethane/TEOS) hybrids as protective coatings: A synergistic approach utilising plant oil polyols, a sustainable resource. *Prog. Org. Coat.* **2017**, *108*, 1−14.
(18) Bhosale, N.; Shaik, A.; Mandal, S. K. Synthesis and characterization of castor oil based hybrid polymers and their polyurethane−urea/silica coatings. *RSC Adv.* **2015**, *5*, 103625−103635.
(19) Fu, C.; Yang, Z.; Zheng, Z.; Shen, L. Properties of alkoxysilane castor oil synthesized via thiol-ene and its polyurethane/siloxane hybrid coating films. *Prog. Org. Coat.* **2014**, *77*, 1241−1248.
(20) de Freitas, B. D.; Onishi, B. S. D.; Caixeta, F. J.; Bortoletto-Santos, R.; Garcia, F. D. R.; Messaddeq, Y.; Ribeiro, S. J. L. Green host urethanesil based on castor oil doped with Eu3+ complex. *Opt. Mater.* **2023**, *138*, 113706.
(21) Pinzón, E. F.; Santos, A. d.; Bueno, P. R. Density of states of a nanoscale semiconductor interface as a transduction signal for sensing molecules. *ACS Appl. Electron. Mater.* **2021**, *3*, 3411−3417.
(22) Pinzón, E. F.; Lopes, L. C.; Fonseca, A. F. V.; Schiavon, M. A.; Bueno, P. R. Quantum rate as a spectroscopic methodology for measuring the electronic structure of quantum dots. *J. Mater. Chem. C* **2024**, *12*, 4606.
(23) Lopes, L. C.; Santos, A.; Bueno, P. R. Measuring quantum conductance and capacitance of graphene using impedance-derived capacitance spectroscopy. *Carbon* **2021**, *184*, 821−827.
(24) Alarcón, E. V. G.; Santos, A.; Bueno, P. R. Perspective on quantum electrochemistry. A simple method for measuring the electron transfer rate constant. *Electrochim. Acta* **2021**, *398*, 139219.
(25) Kerko, D. J.; Morgan, D. W.; Morse, D. L. Photochromic glass compositions for lightweight lenses. U.S. Patent 4,608,349 A, 1986.
(26) Mauro, J. C.; Thirion, L. M. Reverse photochromic borosilicate glasses. WO 2015054346 A1, 2015.
(27) Kim, B.-K.; Deng, J.; Wenjing, X.; Van Gemert, B.; Chopra, A.; Molock, F.; Mahadevan, S. Ophthalmic devices comprising photochromic materials having extended pi-conjugated systems. U.S. Patent 20,060,226,402 A1, 2006.
(28) Tällberg, R.; Jelle, B. P.; Loonen, R.; Gao, T.; Hamdy, M. Comparison of the energy saving potential of adaptive and controllable smart windows: A state-of-the-art review and simulation studies of thermochromic, photochromic and electrochromic technologies. *Sol. Energy Mater. Sol. Cells* **2019**, *200*, 109828.
(29) Su, A.; Grist, S. M.; Geldert, A.; Gopal, A.; Herr, A. E. Quantitative UV-C dose validation with photochromic indicators for informed N95 emergency decontamination. *PLoS One* **2021**, *16*, No. e0243554.
(30) Wen, G.-Y.; Zhou, X.-L.; Tian, X.-Y.; Hu, T.-Y.; Xie, R.; Ju, X.-J.; Liu, Z.; Pan, D.-W.; Wang, W.; Chu, L.-Y. Real-time quantitative detection of ultraviolet radiation dose based on photochromic hydrogel and photo-resistance. *Chem. Mater.* **2022**, *34*, 7947−7958.
(31) Byron, H.; Kreivilä, T.; Colinet, P.; Le Bahers, T.; Lastusaari, M. New shades of photochromism − yellow sodalites for the detection of blue light. *J. Mater. Chem. C* **2023**, *11*, 3360−3374.
(32) Wales, D. J.; Cao, Q.; Kastner, K.; Karjalainen, E.; Newton, G. N.; Sans, V. 3D-printable photochromic molecular materials for reversible information storage. *Adv. Mater.* **2018**, *30*, 1800159.
(33) Lv, Y.; Zhang, S.; Li, Z.; Jin, Y.; Wu, H.; Ju, G.; Chen, L.; Hu, Z.; Hu, Y. Reversible multiplexing optical information storage and photoluminescence switching in Eu^{2+}-doped fluorophosphate-based

tunable photochromic materials. *J. Mater. Chem. C* **2021**, *9*, 5930−5944.
(34) Yamase, T. Photo- and electrochromism of polyoxometalates and related materials. *Chem. Rev.* **1998**, *98*, 307−326.
(35) Gonçalves, L. P.; Ferreira-Neto, E. P.; Ullah, S.; de Souza, L. V.; Ysnaga, O. A. E.; dos Santos, M. V.; Ribeiro, S. J. L.; Rodrigues-Filho, U. P. Enhanced photochromic response of ormosil−phosphotungstate nanocomposite coatings doped with TiO_2 nanoparticles. *J. Sol-Gel Sci. Technol.* **2015**, *76*, 386−394.
(36) Wang, S.; Fan, W.; Liu, Z.; Yu, A.; Jiang, X. Advances on tungsten oxide based photochromic materials: strategies to improve their photochromic properties. *J. Mater. Chem. C* **2018**, *6*, 191−212.
(37) Pardo, R.; Zayat, M.; Levy, D. Photochromic organic-inorganic hybrid materials. *Chem. Soc. Rev.* **2011**, *40*, 672−687.
(38) de Oliveira, M., Jr; de Souza, A. L.; Schneider, J.; Rodrigues-Filho, U. P. Local structure and photochromic response in ormosils containing dodecatungstophosphoric acid. *Chem. Mater.* **2011**, *23*, 953−963.
(39) Cruz, R. P.; Nalin, M.; Ribeiro, S. J. L.; Molina, C. Photochromic dynamics of organic−inorganic hybrids supported on transparent and flexible recycled (PET). *Opt. Mater.* **2017**, *66*, 297−301.
(40) Schubert, U.. In *The Sol-Gel Handbook*; Levy, D., Zayat, M., Eds.; Wiley-VCH Verlag GmbH & Co. KGaA: Weinheim, Germany, 2015; pp 1−28.
(41) Montheil, T.; Echalier, C.; Martinez, J.; Subra, G.; Mehdi, A. Inorganic polymerization: an attractive route to biocompatible hybrid hydrogels. *J. Mater. Chem. B* **2018**, *6*, 3434−3448.
(42) Bokov, D.; Turki Jalil, A.; Chupradit, S.; Suksatan, W.; Javed Ansari, M.; Shewael, I. H.; Valiev, G. H.; Kianfar, E. Nanomaterial by sol-gel method: Synthesis and application. *Adv. Mater. Sci. Eng.* **2021**, *2021*, 5102014.
(43) Mattia, J.; Painter, P. A. comparison of hydrogen bonding and order in a polyurethane and poly(urethane-urea) and their blends with poly(ethylene glycol). *Macromolecules* **2007**, *40*, 1546−1554.
(44) Fu, L.; Ferreira, R. A. S.; Silva, N. J. O.; Fernandes, A. J.; Ribeiro-Claro, P.; Gonçalves, I. S.; Bermudez, V. d. Z.; Carlos, L. D. Structure−photoluminescence relationship in Eu(iii) β-diketonate-based organic−inorganic hybrids. Influence of the synthesis method: carboxylic acid solvolysis versus conventional hydrolysis. *J. Mater. Chem.* **2005**, *15*, 3117.
(45) Fu, L.; Sá Ferreira, R. A.; Fernandes, M.; Nunes, S. C.; de Zea Bermudez, V.; Hungerford, G.; Rocha, J.; Carlos, L. D. Photoluminescence and quantum yields of organic/inorganic hybrids prepared through formic acid solvolysis. *Opt. Mater.* **2008**, *30*, 1058−1064.
(46) Braz, A. G.; Pulcinelli, S. H.; Santilli, C. V. Glycerol-based polyurethane-silica organic-inorganic hybrid as an anticorrosive coating. *Prog. Org. Coat.* **2022**, *169*, 106939.
(47) Wang, W.; Marshall, M.; Collins, E.; Marquez, S.; Mu, C.; Bowen, K. H.; Zhang, X. Intramolecular electron-induced proton transfer and itscorrelation with excited-state intramolecular proton transfer. *Nat. Commun.* **2019**, *10*, 1170.
(48) Petek, H.; Zhao, J. Ultrafast interfacial proton-coupled electron transfer. *Chem. Rev.* **2010**, *110*, 7082−7099.
(49) Bueno, P. R. Quantum rate theory and electron-transfer dynamics: A theoretical and experimental approach for quantum electrochemistry. *Electrochim. Acta* **2023**, *466*, 142950.
(50) Bueno, P. R. On the fundamentals of quantum rate theory and the long-range electron transport in respiratory chains. *Chem. Soc. Rev.* **2024**, *53*, 5348−5365.
(51) Ashcroft, N.; Mermin, N. *Solid State Physics; HRW International*; Holt, Rinehart and Winston, 1976.
(52) Levine, I. *Quantum Chemistry Pearson advanced chemistry series*; Pearson, 2014.
(53) Dieckmann, A.; Bässler, H.; Borsenberger, P. M. An assessment of the role of dipoles on the density-of-states function of disordered molecular solids. *J. Chem. Phys.* **1993**, *99*, 8136−8141.
(54) Vukmirović, N.; Wang, L.-W. Density of states and wave function localization in disordered conjugated polymers: a large scale computational study. *J. Phys. Chem. B* **2011**, *115*, 1792−1797.
(55) Shah, A. A.; Umar, A. A.; Salleh, M. M. Efficient quantum capacitance enhancement in DSSC by gold nanoparticles plasmonic effect. *Electrochim. Acta* **2016**, *195*, 134−142.
(56) Sakr, G. B.; Yahia, I. S. Effect of illumination and frequency on the capacitance spectroscopy and the relaxation process of p-ZnTe/n-CdMnTe/GaAs magnetic diode for photocapacitance applications. *J. Alloys Compd.* **2010**, *503*, 213−219.
(57) Yoo, J.; Nam, Y.; Kim, T.-S.; Jung, G.; Song, J.-H.; Chang, S.-K. Light-induced capacitance enhancement and successive carrier escape in InGaN/GaN multiple quantum wells. *J. Appl. Phys.* **2020**, *127*, 024503.
(58) He, C.; Qiu, S.; Sun, S.; Zhang, Q.; Lin, G.; Lei, S.; Han, X.; Yang, Y. Electrochemically active phosphotungstic acid assisted prevention of graphene restacking for high-capacitance supercapacitors. *Energy Environ. Mater.* **2018**, *1*, 88−95.
(59) Ilbeygi, H.; Kim, I. Y.; Kim, M. G.; Cha, W.; Kumar, P. S. M.; Park, D.-H.; Vinu, A. Highly crystalline mesoporous phosphotungstic acid: a high-performance electrode material for energy-storage applications. *Angew. Chem.* **2019**, *131*, 10965−10970.
(60) Permatasari, A.; Lee, W.; Kwon, Y. Acidic aqueous redox flow battery using 12-phosphotungstic acid and 2, 4, 5, 6-tetrahydroxybenzene-1, 3-disulfonic acid as redox couple. *Int. J. Energy Res.* **2022**, *46*, 13013−13022.
(61) Santos, M. V.; Barud, H. S.; Alencar, M. A. S.; Nalin, M.; Toma, S. H.; Araki, K.; Benedetti, A. V.; Maciel, I. O.; Fragneaud, B.; Legnani, C.; Molina, C.; Cremona, M.; Ribeiro, S. J. L. Self-Supported Smart Bacterial Nanocellulose−Phosphotungstic Acid Nanocomposites for Photochromic Applications. *Front. Mater. Sci.* **2021**, *8*, 668835.
(62) Connell, R.; Keil, J.; Peterson, C.; Hillmyer, M. A.; Ferry, V. E. CdSe/CdS−poly(cyclohexylethylene) thin film luminescent solar concentrators. *APL Mater.* **2019**, *7*, 101123.
(63) D20 Committee. *Test Method for Haze and Luminous Transmittance of Transparent Plastics*, 2021.
(64) Saciloto, T. R.; Cervini, P.; Gomes Cavalheiro, E. T. New screen printed electrode based on graphite and polyurethane composite for the determination of acetaminophen. *Anal. Lett.* **2013**, *46*, 312−322.

https://doi.org/10.1021/acsaelm.5c00826
ACS Appl. Electron. Mater. 2025, 7, 8034−8044